Single-Electron Dynamics of an Atomic Silicon Quantum Dot on the H-Si(100)-(2 × 1) Surface

Marco Taucer,[1,2] Lucian Livadaru,[2] Paul G. Piva,[2] Roshan Achal,[1,3] Hatem Labidi,[1,3] Jason L. Pitters,[3] and Robert A. Wolkow[1,2,3,*]

[1]*Department of Physics, University of Alberta, Edmonton, Alberta, Canada T6G 2E1*

[2]*Quantum Silicon, Inc., Edmonton, Alberta, Canada T6G 2M9*

[3]*National Institute for Nanotechnology, National Research Council of Canada, Edmonton, Alberta, Canada T6G 2M9*

(Received 27 January 2014; published 26 June 2014)

Here we report the direct observation of single electron charging of a single atomic dangling bond (DB) on the H-Si(100)-2 × 1 surface. The tip of a scanning tunneling microscope is placed adjacent to the DB to serve as a single-electron sensitive charge detector. Three distinct charge states of the dangling bond—positive, neutral, and negative—are discerned. Charge state probabilities are extracted from the data, and analysis of current traces reveals the characteristic single-electron charging dynamics. Filling rates are found to decay exponentially with increasing tip-DB separation, but are not a function of sample bias, while emptying rates show a very weak dependence on tip position, but a strong dependence on sample bias, consistent with the notion of an atomic quantum dot tunnel coupled to the tip on one side and the bulk silicon on the other.

DOI: 10.1103/PhysRevLett.112.256801 PACS numbers: 73.63.Kv, 73.20.Hb

Quantum dots are a building block for a range of candidate technologies. Single electrons can be trapped and manipulated in single- or multiple-quantum dot structures which allows control over occupation down to single electrons [1,2], single-electron charge detection [3,4], and coherent control of both spatial wave functions [5,6] and spin states [7–9]. Schemes for employing quantum dot systems have been developed to the level of architectures for both classical [10,11] and quantum [12] information applications. A drawback of most quantum dot systems is the need for cryogenic temperatures, a straightforward consequence of the relatively small charging energies of the quantum dots. As quantum dots are miniaturized, charging energies are increased. Ultimately miniaturized quantum dots are embodied in atomic impurities and atom-scale defects, and these are giving birth to a new arena for technological progress. Recent work on embedded impurities in Si has delivered impressive single-electron devices, demonstrating a single atom single-electron transistor (SET) [13], coherent spin control [14], and optical addressing of single atoms [15,16]. Currently, embedded impurities cannot be placed with atom-scale precision, which is a fundamental limitation for some applications [17]. By contrast, dangling bonds (DBs) on the Si surface can be fabricated with truly atomic precision [18,19], and are thus an attractive candidate for atomic quantum dots.

On the H-Si(100)-2 × 1 surface, DBs are isolated sp^3 orbitals that do not participate in chemical bonding, and introduce within the band gap a single surface state. Single DBs exist where there is a single hydrogen atom missing from an otherwise hydrogen-terminated surface. Localization of charge, variable occupation, strong Coulomb interaction, and the possibility of creating tailor-made structures including tunnel coupling between DBs, leads to a description of DBs as atomic silicon quantum dots (ASiQDs). There is a body of theoretical work exploring the possibility of using DBs as building blocks for transport and logic devices [20–23]. The potential of using DBs to create functional device elements with tailor-made electronic properties is only just being explored and understood [19,24,25], and likewise fabrication is now being optimized (and commercialized) [26–28].

The DB energy levels have been estimated using density functional theory (DFT), which places the neutral state, DB^0, at 0.35 eV and the negative state, DB^-, at 0.85 eV above the valence band (VB) [23,29] (Fig. 1). Although there are three distinct charge states, we only refer to two energy levels in this manuscript, the so-called neutral and negative energy levels, also referred to as the $+/0$ and $0/-$ transition levels, respectively. A binding energy is sometimes attributed to the DB^+ state [25], but since there is no associated transition level, its energy level is inaccessible in spectroscopy.

Despite the central role of single-electron dynamics in STM imaging of DBs [30–32] as well as in potential DB-based atom-scale devices [22], until now, they have not been directly observed in an STM experiment. Here, we report direct observation of single-electron charging dynamics of DBs. The dynamics are consistent with a model of nonequilibrium charging, in which the DB acts as the island of an SET, tunnel coupled to the STM tip and to the Si bulk. The variably charged DB has a gating effect on the tip-sample tunnel junction, so that the total tunneling current acts as a single-electron sensitive charge sensor.

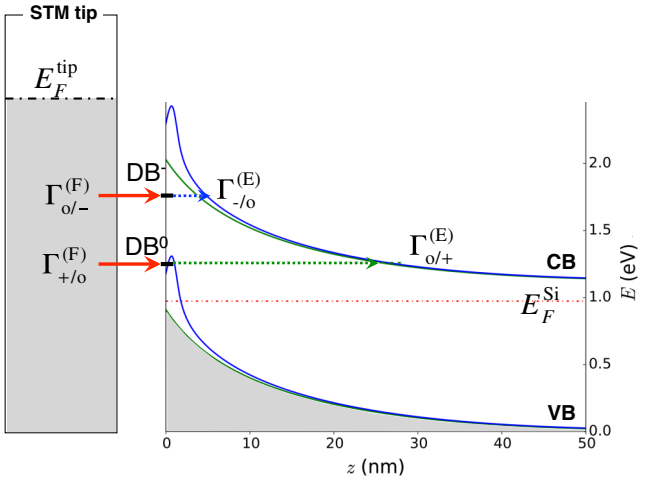

FIG. 1 (color online). Band diagram representing the nonequilibrium dynamics of STM imaging of a DB. E_F^{tip} and E_F^{Si} label the tip and sample chemical potentials, respectively, and Γ labels filling and emptying processes. TIBB was calculated using the SEMITIP code [36] assuming typical STM experimental parameters and resulting bands are shown as green curves, corresponding to the case of DB^0. For the case of DB^-, combined tip- and DB-induced band bending (shown as blue curves) are calculated using a Slater-type orbital for the DB [31] assuming also that dynamic screening effects in the sample are negligible.

In this experiment, the DB does not act as a current-carrying state: a negligible fraction of the current passes through the DB. The tip Fermi level is at all times higher in energy than both transition levels. Thus, this experiment allows observation of the three DB charge states, whereas more familiar scanning tunneling spectroscopy experiments would be fundamentally limited to observations of the two transition levels.

For these experiments, we used an Omicron LT-STM operated at 4.2 K. The tungsten tip was prepared by electrochemical etching followed by electron beam heating and field ion microscopy cleaning and sharpening [33]. The sample was cleaved from a 3–4 m$\Omega \cdot$ cm n-type As-doped Si(100) wafer and was cleaned by heating several times to roughly 1250 °C, and H-terminated at 330 °C [34]. The high temperatures used to clean the sample are known to deplete the dopants near the surface [35].

The sharply defined dark region which is known to surround DBs in unoccupied state imaging is known as a "halo" (e.g., see previous studies [18,25,31] and Fig. 2 of the Supplemental Material [37]). DB halos have been attributed to upward band bending near a negatively charged DB. A theory of STM of DBs which captures the qualitative features of the topography of DB halos was put forth by Livadaru *et al.* [31]. In unoccupied state imaging, tip-induced band bending (TIBB) tends to empty nearby states (including the DB). At the same time, electrons tunnel from the tip to the unoccupied sample energy levels. When an electron is injected into a localized state, the dynamics which would re-establish thermal equilibrium in the sample can be relatively slow, and the equilibrium picture of STM no longer applies. According to this nonequilibrium picture of STM imaging of DBs, the charge state of the DB is determined by the competition of filling and emptying processes, as shown in Fig. 1.

At low temperature, many thermal processes become negligible, and dynamics can be slow enough to be within the STM preamplifier bandwidth. Figure 2(a) shows a topographical unoccupied state image of a DB at 4.2 K. At these conditions, the edge of the halo is no longer sharp, but instead shows a distinctive streaky noise. When the tip is positioned in the halo region, and the tip height is held constant, the measurement of current as a function of time shows unusual jumps to discrete values, as seen in Fig. 2(c). Such current steps are absent when the tip is far from any DBs. The histogram of current measurements shown in Fig. 2(b) demonstrates that there are precisely three dominant current values. We identify these as corresponding to the negative (doubly occupied), neutral (singly occupied), and positive (unoccupied) charge states of the DB. Each charge state of the DB causes a different DB-induced band bending under the tip apex, and thereby creates a different current from tip to sample.

The electron dynamics represented in Figs. 2(b) and (c) are for a particular tip position and voltage, but in general the dynamics and probabilities of the three charge states will depend on these parameters. Each panel in Fig. 3

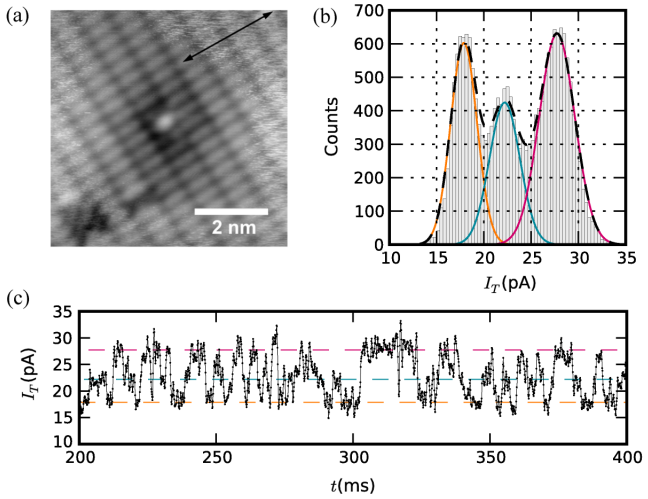

FIG. 2 (color online). (a) Topographical STM image of a single DB taken with $V_S = 1.4$ V and $I_T = 20$ pA. The double-ended arrow shows the range of lateral positions used to acquire the data shown in Fig. 3. (b) Histogram of current measurements with the tip at a constant height and a constant voltage of $V_S = 1.45$ V positioned 3.14 nm from the DB. The peak at lowest current corresponds to the negative charge state, while the peaks at intermediate and highest current correspond to the neutral and positive charge states. (c) An example of a current-time trace. The sampling rate is 10 kHz and the entire trace (not shown) is 2 s in length.

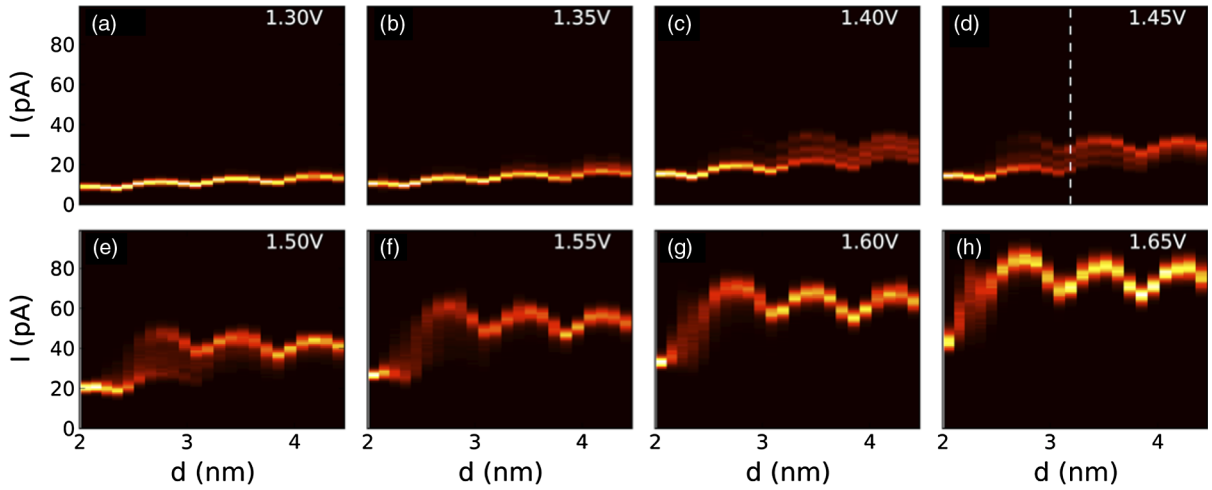

FIG. 3 (color online). Color maps showing frequency of current measurements as a function of tip-DB separation and current from (a) 1.30 to (h) 1.65 V. Color map intensity is proportional to the number of instances of a particular measurement of current at a particular position. Any vertical slice of any color map gives a histogram whose total integral is 2 s × 10 kHz = 20 000 samples. In particular, the dotted line in (d) corresponds to the data shown in Fig. 2(b).

compactly shows a collection of histograms at different lateral positions crossing the edge of a DB halo, for a particular tip voltage. Color map intensity is proportional to the number of counts at a particular current and tip-DB separation, and tip height is constant for all the data presented. At all voltages there is a periodic modulation in current as a function of position, due to the surface topography; as the tip moves laterally at constant height, the tip-sample distance is modulated because of the periodicity of the Si surface. The striking feature is the appearance of current instability reflected by the broadening and/or existence of multiple current levels at particular voltages and positions.

At the lowest sample voltage (Fig. 3(a) at 1.30 V), the DB is in a single charge state at all tip positions. The STM current decreases as the tip moves toward the DB (aside from the above-mentioned periodic modulation due to topography), indicating upward band bending near the DB, consistent with a negative charge state. As the tip bias is increased [Figs. 3(b)–(h)], two additional charge states become visible, which we identify as the neutral and positive DB states. For voltages greater than 1.35 V, there is a transition region in which all three charge states are visible, with the positive DB charge state becoming dominant at larger tip-DB separations. Above 1.50 V, transitions occur on a time scale which competes with the data acquisition rate, so that the three states become blurred and eventually averaged. At 1.55 V and above, the high-current peak dominates for most tip positions, and here we see that current *increases* as the tip moves toward the DB, indicating *downward* band bending near the DB, consistent with a positive charge state. All traces show a low-current value at the smallest tip-DB separation because direct tunneling from the tip to the DB becomes dominant, in turn causing negative charging of the DB.

Looking at Fig. 2(c) we can see that the $I(t)$ traces contain dynamical information; the traces consist of plateaus of various lengths, and the dynamics can in principle be extracted by measuring their lengths as well as which states they transition to. This would give the transition rates, $\Gamma^{(E)}_{-/0}$, $\Gamma^{(E)}_{0/+}$, $\Gamma^{(F)}_{0/-}$, and $\Gamma^{(F)}_{+/0}$, for the kinetic scheme

$$\mathrm{DB}^- \underset{\Gamma^{(F)}_{0/-}}{\overset{\Gamma^{(E)}_{-/0}}{\rightleftharpoons}} \mathrm{DB}^0 \underset{\Gamma^{(F)}_{+/0}}{\overset{\Gamma^{(E)}_{0/+}}{\rightleftharpoons}} \mathrm{DB}^+,$$

which assumes that there is no direct transition between the negative state and positive state, thus neglecting any particular two-electron filling or emptying processes. The superscripts (F) and (E) indicate filling and emptying rates. Determining these rates by simply measuring the lengths of plateaus in Fig. 2(c) turns out to be problematic, since the noise in the plateaus is comparable with their separation. Motivated by this, we take an approach developed by Hoffmann and Woodside [38] called signal-pair analysis, which considers the evolution of subsets of a data set for a current-time trace chosen to initially belong to a particular charge state, fitting their evolving distributions using a dynamical model, and thereby extracting the transition rates between states even if their signals overlap significantly. This analysis combines earlier work on single-molecule fluorescence studies [39], and a signal-pair correlation approach to analyzing structural dynamics of proteins [40]. The procedure is explained in the Supplemental Material [37].

The extracted filling and emptying rates for sample biases of 1.40, 1.45, and 1.50 V, are shown in Fig. 4. At higher biases, dynamics could not be extracted because the transition rates were faster than the preamplifier

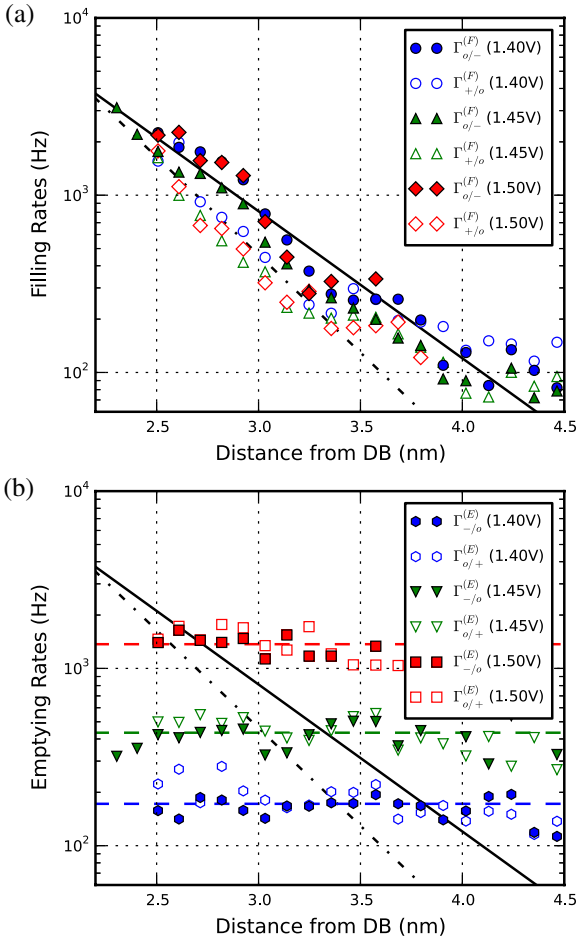

FIG. 4 (color online). (a) Experimentally measured filling rates as a function of lateral tip distance from DB for three different voltages. The dashed dotted line indicates the exponential fit to the filling rate of the neutral DB energy level, while the solid line indicates the fit for the negative DB level. (b) Experimentally measured emptying rates as a function of lateral tip distance from DB for three different voltages. For each voltage, emptying rates have a weak dependence on tip position. The dashed colored lines show the average emptying rate for each voltage, while the dashed-dotted and solid black lines show the same fits to the filling rates as shown in (a).

bandwidth. At lower voltages, the DB tended to stay in the negative charge state at all tip positions, again making it impossible to extract the dynamics.

Figure 4(a) shows the dependence of filling rates on tip position for three different voltages. There is an exponential decay in the filling rate with increasing tip-DB separation, with values from roughly 3 kHz to 50 Hz, with no clear systematic dependence of filling rates on voltage. This is consistent with the prediction that direct tunneling from tip to DB dominates the filling of the DB, assuming a constant density of tip states over the energy range of interest. The exponential fits to the filling rates of the neutral and negative charge states are shown as a black dashed-dotted line and a black solid line, respectively. Their decay rates are $k^{(F)}_{0/-} = 1.91$ and $k^{(F)}_{+/0} = 2.54$ nm^{-1}. We attribute the slower decay of $\Gamma^{(F)}_{0/-}$ to the upward shift of the DB$^-$ energy level with respect to that of DB^0, resulting in a smaller ionization potential, and a slower decay of the DB$^-$ wave function into vacuum.

Figure 4(b) shows emptying rates. In contrast to Fig. 4(a), we see a strong voltage dependence and a very weak position dependence. The average emptying rate for each of the three voltages is shown as a horizontal dashed line. We find relatively flat emptying rates of 172, 434, and 1369 Hz for sample voltages of 1.40, 1.45, and 1.50 V respectively. While calculations for DBs at room temperature [31] found thermal emission of electrons to dominate emptying in unoccupied-state STM imaging, this process is virtually eliminated at 4.2 K. We instead consider the dominant mechanism at low temperature to be tunneling from the DB energy level to distant resonant conduction band (CB) levels. As the bias is increased, TIBB is also increased, while the associated barrier for an electron on the DB to tunnel to the CB becomes narrower. The weak dependence of emptying rates on lateral tip position is an indication that TIBB is relatively uniform on the scale considered here, as expected.

We can now see that the edge of the DB halo is the point at which filling rates overtake emptying rates. This corresponds to the intersection of the horizontal dashed lines (emptying) in Fig. 4(b) with the exponential solid and dashed dotted lines (filling). As voltage is increased, the emptying rate, which is nearly flat with respect to position, increases while the filling rate remains an unchanged exponential. The point of intersection (edge of the halo) thus moves toward the DB. This is consistent with our routine observation of a DB halo size which decreases with increasing bias (not shown). Beyond the dependence of rates on bias and tip-DB lateral separation, we see that both filling rates are similar in magnitude, as are both emptying rates. At this time, a quantitative study is not permitted by the data we can acquire, but a more detailed discussion of the orbitals and band bending effects associated with DB^0 and DB$^-$ is provided in the Supplemental Material [37].

In conclusion, we have shown that single-electron dynamics are directly observable in STM of single DBs when the tunnel junction between the tip and the sample acts as a single-electron sensitive charge detector. We directly resolve the three possible charge states—negative, neutral, and positive—of a DB. The dynamics extracted from current traces are consistent with a nonequilibrium model in which the DB acts as an atomic quantum dot, tunnel coupled both to the tip and to the bulk Si, and occupation is determined by the competition of filling from the tip and emptying to the bulk. These results show that the charge state of an atomic quantum dot can be manipulated and read by nearby electrodes. There is no fundamental reason why the single atom charge state sensing

demonstrated here cannot in the future be implemented in an STM-free, lithographic structure.

We would like to thank Armin Hoffmann and Michael Woodside for very valuable discussions and Martin Cloutier and Mark Salomons for their technical expertise.

*Corresponding author.
rwolkow@ualberta.ca

[1] M. Ciorga, A. S. Sachrajda, P. Hawrylak, C. Gould, P. Zawadzki, S. Jullian, Y. Feng, and Z. Wasilewski, Phys. Rev. B **61**, R16315 (2000).
[2] C. B. Simmons, M. Thalakulam, N. Shaji, L. J. Klein, H. Qin, R. H. Blick, D. E. Savage, M. G. Lagally, S. N. Coppersmith, and M. A. Eriksson, Appl. Phys. Lett. **91**, 213103 (2007).
[3] M. Field, C. G. Smith, M. Pepper, D. A. Ritchie, J. E. F. Frost, G. A. C. Jones, and D. G. Hasko, Phys. Rev. Lett. **70**, 1311 (1993).
[4] L. Gaudreau, S. A. Studenikin, A. S. Sachrajda, P. Zawadzki, A. Kam, J. Lapointe, M. Korkusinski, and P. Hawrylak, Phys. Rev. Lett. **97**, 036807 (2006).
[5] K. D. Petersson, J. R. Petta, H. Lu, and A. C. Gossard, Phys. Rev. Lett. **105**, 246804 (2010).
[6] M. Korkusinski, I. P. Gimenez, P. Hawrylak, L. Gaudreau, S. A. Studenikin, and A. S. Sachrajda, Phys. Rev. B **75**, 115301 (2007).
[7] L. Gaudreau, G. Granger, A. Kam, G. C. Aers, S. A. Studenikin, P. Zawadzki, M. Pioro-Ladrière, Z. R. Wasilewski, and A. S. Sachrajda, Nat. Phys. **8**, 54 (2011).
[8] M. Busl, G. Granger, L. Gaudreau, R. Sánchez, A. Kam, M. Pioro-Ladrière, S. A. Studenikin, P. Zawadzki, Z. R. Wasilewski, A. S. Sachrajda, and G. Platero, Nat. Nanotechnol. **8**, 261 (2013).
[9] H. Ribeiro, G. Burkard, J. R. Petta, H. Lu, and A. C. Gossard, Phys. Rev. Lett. **110**, 086804 (2013).
[10] C. S. Lent, P. D. Tougaw, W. Porod, and G. H. Bernstein, Nanotechnology **4**, 49 (1993).
[11] L. Lu, W. Liu, and M. O'Neill, IEEE Trans. Comput. **62**, 548 (2013).
[12] D. Loss and D. P. DiVincenzo, Phys. Rev. A **57**, 120 (1998).
[13] M. Fuechsle, J. A. Miwa, S. Mahapatra, H. Ryu, S. Lee, O. Warschkow, L. C. L. Hollenberg, G. Klimeck, and M. Y. Simmons, Nat. Nanotechnol. **7**, 242 (2012).
[14] A. Morello, J. J. Pla, F. A. Zwanenburg, K. W. Chan, K. Y. Tan, H. Huebl, M. Möttönen, C. D. Nugroho, C. Yang, J. A. van Donkelaar, A. D. C. Alves, D. N. Jamieson, C. C. Escott, L. C. L. Hollenberg, R. G. Clark, and A. S. Dzurak, Nature (London) **467**, 687 (2010).
[15] C. Yin, M. Rancic, G. G. de Boo, N. Stavrias, J. C. McCallum, M. J. Sellars, and S. Rogge, Nature (London) **497**, 91 (2013).
[16] E. P. Smakman, J. van Bree, and P. M. Koenraad, Phys. Rev. B **87**, 085414 (2013).
[17] B. Kane, MRS Bull. **30**, 105 (2005).
[18] M. B. Haider, J. L. Pitters, G. A. DiLabio, L. Livadaru, J. Y. Mutus, and R. A. Wolkow, Phys. Rev. Lett. **102**, 046805 (2009).
[19] J. L. Pitters, L. Livadaru, M. B. Haider, and R. A. Wolkow, J. Chem. Phys. **134**, 064712 (2011).
[20] Z. Shaterzadeh-Yazdi, L. Livadaru, M. Taucer, J. Y. Mutus, J. L. Pitters, R. A. Wolkow, and B. C. Sanders, Phys. Rev. B **89**, 035315 (2014).
[21] R. Robles, M. Kepenekian, S. Monturet, C. Joachim, and N. Lorente, J. Phys. Condens. Matter **24**, 445004 (2012).
[22] H. Kawai, F. Ample, Q. Wang, Y. K. Yeo, M. Saeys, and C. Joachim, J. Phys. Condens. Matter **24**, 095011 (2012).
[23] L. Livadaru, P. Xue, Z. Shaterzadeh-Yazdi, G. A. DiLabio, J. Mutus, J. L. Pitters, B. C. Sanders, and R. A. Wolkow, New J. Phys. **12**, 083018 (2010).
[24] A. Bellec, L. Chaput, G. Dujardin, D. Riedel, L. Stauffer, and P. Sonnet, Phys. Rev. B **88**, 241406 (2013).
[25] S. R. Schofield, P. Studer, C. F. Hirjibehedin, N. J. Curson, G. Aeppli, and D. R. Bowler, Nat. Commun. **4**, 1649 (2013).
[26] K. E. J. Goh, S. Chen, H. Xu, J. Ballard, J. N. Randall, and J. R. Von Ehr, Appl. Phys. Lett. **98**, 163102 (2011).
[27] S. Chen, H. Xu, K. E. J. Goh, L. Liu, and J. N. Randall, Nanotechnology **23**, 275301 (2012).
[28] M. Kolmer, S. Godlewski, R. Zuzak, M. Wojtaszek, C. Rauer, A. Thuaire, J.-M. Hartmann, H. Moriceau, C. Joachim, and M. Szymonski, Appl. Surf. Sci. **288**, 83 (2014).
[29] See M. Baseer Haider, J. L. Pitters, G. A. DiLabio, L. Livadaru, J. Y. Mutus, and R. A. Wolkow, arXiv:0807.0609 for further details of DFT calculations.
[30] M. Berthe, R. Stiufiuc, B. Grandidier, D. Deresmes, C. Delerue, and D. Stiévenard, Science **319**, 436 (2008).
[31] L. Livadaru, J. L. Pitters, M. Taucer, and R. A. Wolkow, Phys. Rev. B **84**, 205416 (2011).
[32] T. H. Nguyen, G. Mahieu, M. Berthe, B. Grandidier, C. Delerue, D. Stiévenard, and P. Ebert, Phys. Rev. Lett. **105**, 226404 (2010).
[33] M. Rezeq, J. L. Pitters, and R. A. Wolkow, J. Chem. Phys. **124**, 204716 (2006).
[34] J. J. Boland, Adv. Phys. **42**, 129 (1993).
[35] J. L. Pitters, P. G. Piva, and R. A. Wolkow, J. Vac. Sci. Technol. B **30**, 021806 (2012).
[36] R. M. Feenstra, J. Vac. Sci. Technol. B **21**, 2080 (2003).
[37] See the Supplemental Material at http://link.aps.org/supplemental/10.1103/PhysRevLett.112.256801 for a detailed description of the data analysis and for additional experimental results at room temperature.
[38] A. Hoffmann and M. T. Woodside (personal communication).
[39] A. Hoffmann, D. Nettels, J. Clark, A. Borgia, S. E. Radford, J. Clarke, and B. Schuler, Phys. Chem. Chem. Phys. **13**, 1857 (2011).
[40] A. Hoffmann and M. T. Woodside, Angew. Chem., Int. Ed. Engl. **50**, 12643 (2011).